



ELSEVIER

Available online at www.sciencedirect.com

Journal of Materials Research and Technology

journal homepage: www.elsevier.com/locate/jmrt**Original Article****Influence of SiC reinforcement on microstructural and thermal properties of SAC0307 solder joints**

Agata Skwarek ^{a,b,*}, Balázs Illés ^c, Paweł Górecki ^b, Adrian Pietruszka ^b, Jacek Tarasiuk ^d, Tamás Hurtony ^c

^a Lukasiewicz Research Network-Institute of Microelectronics and Photonics, Zablocie 39, 30-701 Kraków, Poland

^b Gdynia Maritime University, Morska 81-87, 81-225 Gdynia, Poland

^c Budapest University of Technology and Economics, Egry 18, Budapest, Hungary

^d AGH-University of Science and Technology, 30-059 Kraków, Poland

ARTICLE INFO**Article history:**

Received 5 August 2022

Accepted 20 November 2022

Available online 25 November 2022

Keywords:

Composite solder

SiC

Nano-particles

Nano-fiber

Microstructural refinement

Thermal parameters

ABSTRACT

The effect of SiC nano-phases (nano-particles and nano-fibers) addition into SAC0307 solder paste was investigated on the thermal and microstructural properties of the composite solder joints. The nano-phases were used between 0.125 and 1 wt%, and they were mixed into the solder paste by ball milling process. For the study power MOSFET (metal oxide semiconductor field effect transistor) components were soldered onto metal core printed circuit boards (MCPCBs). The thermal impedance $Z_{th}(t)$ and thermal resistance R_{th} of MOSFETs were measured by an indirect electrical method. Furthermore, the void formation and the microstructure of solder joints were also studied. The solderability and voiding properties of the composite solder alloys were acceptable. It was found that in 0.5 wt% amount, SiC nano-particles have positive effects on the thermal parameters of the solder joints, which could be explained by the IMC (intermetallic compound) layer growth suppression effect of the nano-phases. The microstructural analysis revealed that the microstructural refinement of the composite solder joints differs in the case of nano-particles and nano-fibers.

© 2022 The Author(s). Published by Elsevier B.V. This is an open access article under the CC BY-NC-ND license (<http://creativecommons.org/licenses/by-nc-nd/4.0/>).

1. Introduction

Modern electronic equipment is essential in every area of our life. One of the main processes of joining electronic components into a functional circuit is still soldering. Nowadays, a research trend aims to reduce the Ag content in SnAgCu solder alloys due to its high price and possible thermo-mechanical problems like solder cracking [1]. Due to the recent intensive

development of power electronics – like inverters in solar energy harvesting systems or power LEDs (light emitting diodes) – there is a strong need for solder joints with good thermal properties and high reliability. To reach this purpose, different kinds of metals, ceramics, IMCs (intermetallic compounds) have been chosen as reinforcements of solder alloy and create composite solder joints. A wide range of ceramic particles has already been used as reinforcement for lead-free solder alloys, like TiO_2 , ZnO , SiC , ZrO_2 , Al_2O_3 , Fe_2O_3 , Si_3Ni_4 , La_2O_3 , etc. [2–6].

* Corresponding author.

E-mail address: agata.skwarek@imif.lukasiewicz.gov.pl (A. Skwarek).

<https://doi.org/10.1016/j.jmrt.2022.11.126>

2238-7854/© 2022 The Author(s). Published by Elsevier B.V. This is an open access article under the CC BY-NC-ND license (<http://creativecommons.org/licenses/by-nc-nd/4.0/>).

Usually, the reinforcements positively affect the quality of the solder joints. However, the non-soluble ceramic particles may slightly increase the liquidus temperature, about 1–2K, of the composite alloy [7].

In the case of SnAgCu systems, the solder joint is built up from β -Sn grains, Cu_6Sn_5 , Cu_3Sn , and Ag_3Sn IMC grains. The reinforcing particles should be small-sized and form self-organized dispersive systems, which promote heterogeneous nucleation. The most important effect of the reinforcement particles is that they change the mechanical and partially the thermal behavior of the solder joints [8,9]. The non-soluble nano-phases incorporate at the grain boundaries into the solder matrix and limit the grain growth (in the case of β -Sn grains and IMC as well) [10–12] and retard the dislocation motion leading finally to solder joint strengthening [13,14]. Liquidus temperature, yield strength, and ultimate tensile strength could increase significantly with the addition of nano-sized particles. On the other side, reinforcement particles can deteriorate the microstructure of the β -Sn matrix and cause solid-solution hardening as well [15–18].

The SiC is a low-cost and easily accessible material because it is a basic substance of semiconductor production [19,20]. It was proven before that the application of SiC could be useful in soldering technology. Liu et al. [21] added 0.05 wt% SiC nano-particles into Sn-3.8Ag-0.7Cu solder, and they observed considerable β -Sn and IMC grain size and spacing decrease, which resulted in 44% improvement in microhardness of the composite solder joints. Wang et al. [22] reinforced Sn-3.7Ag-0.9Zn solder with SiC particles and observed that the microstructure refinement could obstruct the dislocation slipping and thus lead to a strong strengthening effect in the composite solders. El-Daly et al. [2] investigated not only the effect of SiC nano-particles on Sn-1.0Ag-0.5Cu (SAC105) but also [23] Sn-3.0Ag-0.5Cu (SAC305) solder and they found that the addition of SiC effectively reduced the undercooling and pasty range, while the melting temperature is maintained at the SAC(105) level. In a further study, El-Daly et al. [24] proved that SiC nano-particles can effectively increase the primary β -Sn phase and decrease the percentage of Ag_3Sn and Cu_6Sn_5 IMCs in the solder bulk, which IMCs produce a weak interface with the β -Sn matrix.

Kim et al. [25] successfully used SiC nano-particles in Sn–Ag–Bi–In low melting point solder alloy to improve the electron migration reliability of the composite solder alloy in high current stress. El-Daly et al. [15] searched the optimal amount of SiC addition (between 0.35 and 0.75 wt%) into SAC105 solder alloy, and they got the best microstructural properties with 0.35 wt%. The effectiveness was reduced when 0.75% SiC addition started constricting the growth Ag_3Sn and Cu_6Sn_5 IMC and forming a weak interface with the enlarged β -Sn matrix. Wu et al. [26] successfully soldered SiC ceramics with non-eutectic Zn–5Al–3Cu and eutectic Zn–5Al solder alloys by the assistance of ultrasound. In the case of Zn–5Al–3Cu solder alloy, they got a fully grain-refined structure in the bond layer as the ultrasonic action time increased. Pal et al. [27] covered the SiC micro-particles (1–3 μm) with electroless nickel and added them into SAC305 by the powder metallurgy at the level of 0–1.5 wt%. They observed the optimal microstructural and mechanical properties at 1 wt%. Pal et al. [28] have also

observed that the relative contact perimeter and the wettability of the SAC305 composite were significantly improved.

Li et al. [29] incorporated various mass fractions (0, 0.2, 0.4, 0.6, 0.8, 1.0 wt%) of SiC nano-fibers into pure Sn solder. The results demonstrated that the wettability of Sn–xSiC/Cu solder had a significant improvement at 0.6 wt%, and excessive additives would degrade the wettability of the composite solder. However, the Cu_6Sn_5 IMC formation decreased only after doping with 0.8 wt% and more. They tested the behavior of the Cu_6Sn_5 IMC layer in Sn-0.6SiC/Cu system under isothermal aging (250 h) and thermal cycling (1500 cycles), and observed that SiC could suppress the IMC layer growth in the solid phase as well [30]. Yin et al. [31] doped the low silver Sn-0.3Ag-0.7Cu (SAC0307) solder alloy with SiC nano-particles between 0 and 0.1 wt%. They observed the improvement of wettability and reduction of IMC layer thickness with increasing SiC content. However, the IMC grains were refined only when the SiC content was less than 0.06 wt%, over it agglomerated SiC and brittle Ag_3Sn IMC appeared. Pal et al. [32] have also studied the IMC layer growth SAC305-SiC 1 wt% composite solder alloy at different reflow temperatures (230–290 °C). They found an increased IMC layer thickness with the increase in the reflow temperature. Furthermore, micro-cracks were detected at the Cu/SAC interface and in the Cu_6Sn_5 layer, which could cause risks of thermo-mechanical reliability.

Consequently, the application of SiC nano-particles is promising for soldering technology. However, there is no agreement in the literature on which form of SiC nano-phases (particles or fibers) and which amount of it is favorable. Furthermore, most of the previous studies have investigated only composite solder bulks and not real working solder joints in circuits. Therefore, this work aimed to characterize the thermal and microstructural properties of different SACX0307-SiC composite solder alloys prepared from SiC nano-particles and nano-fibers between 0.125 and 1 wt% with solder joints of power MOSFET (metal oxide semiconductor field effect transistor) components to learn more about the applicability of SiC nano-phases in soldering technology.

2. Materials and methods

Composite solder alloys were produced from SACX0307 (Sn99Ag0.3Cu0.7, Alpha Industries) solder paste and SiC nano-particles (Sigma Aldrich 594,911) and SiC nano-fibers (Sigma Aldrich 776,742) using the ball milling process. The particle size/diameter of the SiC nano-particles was below 100 nm. The nano-fibers had the following structure: diameter (D) < 2.5 μm and length/diameter ratio (L/D) ≥ 20. Structural information of the nano-phases was provided by the manufacturer. The nano-phases were used in 0.125, 0.25, 0.5, 0.75, and 1 wt%. The mixing process was carried out for 10 min at 300 rpm using a planetary ball mill Pulverisette 5 to obtain a homogeneous distribution of the nano-phases in the solder paste. Table 1 shows the investigated sample types.

The electrical, thermal, and soldering properties of the solder pastes were tested with MOSFET transistors IPB090N06N3, package TO-263. The components had Ni/Au surface finishes on the leads. These power components were

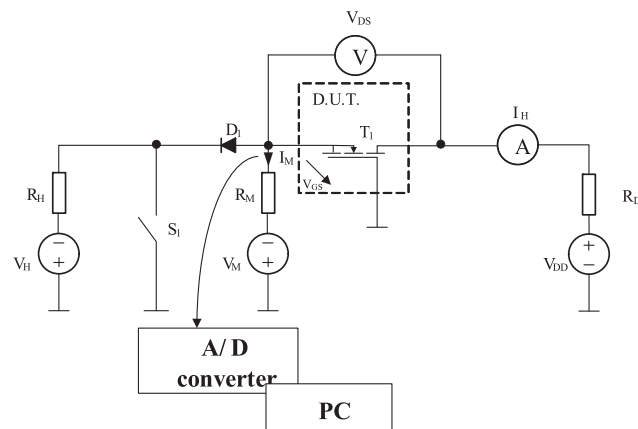
Table 1 – Sample compositions and types.

Solder alloy	Nano-phase type	Amount of nano-phase [wt%]	Samples name abbreviations
SAC0307	—	—	Ref.
SAC0307	nano-particles	0.125	SAC-0.125SiC(p)
SAC0307	nano-particles	0.25	SAC-0.25SiC(p)
SAC0307	nano-particles	0.50	SAC-0.5SiC(p)
SAC0307	nano-particles	0.75	SAC-0.75SiC(p)
SAC0307	nano-particles	1	SAC-1SiC(p)
SAC0307	nano-fibers	0.125	SAC-0.125SiC(f)
SAC0307	nano-fibers	0.25	SAC-0.25SiC(f)
SAC0307	nano-fibers	0.50	SAC-0.5SiC(f)
SAC0307	nano-fibers	0.75	SAC-0.75SiC(f)
SAC0307	nano-fibers	1	SAC-1SiC(f)

soldered onto metalcore substrates (MCPBCB), having a thickness of 1.50 mm, and covered with a 35 μm thick Cu layer. The solder paste was deposited by stencil printing with a stencil thickness of 125 μm . The samples were soldered in an IR (infrared) batch oven with a linear thermal profile (pre-heating 150–180 °C, reflowing 210–254 °C, cooling down 254–170 °C). Seven samples were produced from each type.

The specific thermal conductivity of the SiC filler (360W/m.K [33]) is significantly higher than that of the SAC0307 solder alloy (~60W/m.K). So it could be assumed that the addition of SiC increases the thermal conductivity, but in composite materials, it is not as straightforward. Not only the specific thermal conductivity of the additive is important, but also the geometric orientation of the additive in the matrix. If the additives are oriented parallelly to the heat flow direction, the thermal conductivity is usually improved [34]. However, in the case of non-oriented additives (like in our study), the opposite effect or no effect is also possible [35]. In the macroscopic scale, the non-oriented arrangement of the additives results in local changes in the thermal conductivity of the composite material. This could cause significant calculation errors using commonly applied compact thermal models [34]. Basically, the measurement of the transient thermal impedance of nano-phases would be the best metric for analyzing the thermal properties of the composite solder joints. However, in the case of nano-sized phases, the thermal time constants are very short (nanoseconds) and are hardly measurable. In such a case, mostly simple thermal conductivity is used for the characterization.

Therefore, the effect of the SiC nano-phases on the thermal parameters of the composite solder joints was investigated by indirect electrical measurement (Fig. 1) [36], and the effect of the uneven distribution of the additives in the composite solder joints was investigated statistically. First, the transient thermal impedance Z_{th} [K/W] of the samples was measured, and the thermal resistance R_{th} [K/W] values were calculated from the Z_{th} measurements (as the value of the thermal steady-state). An indirect electrical method was used based on gate-emitter voltage V_{GE} as a thermosensitive parameter. The $V_{GE}(T)$ dependence was characterized by a high slope in the saturation range of the measured curves, which results in a high resolution of $Z_{\text{th}}(t)$ measurements. During the measurements, the assembly was fixed to a liquid-cooled heat exchanger to increase the cooling efficiency.

**Fig. 1 – Transient thermal impedance $Z_{\text{th}}(t)$ measurement set-up.**

During the measurements, V_{DD} and V_H sources provided the transistor saturation bias during its heating (when the switch S_1 is open). After reaching the thermal steady state of the transistor, the values of the voltage V_{DS} and the current I_D were recorded. After switch S_1 was closed, the transistor polarity was provided by the sources V_{DD} and V_M while ensuring the flow of the test current I_M through the transistor drain. This step records the voltage waveform $V_{GS}(t)$ until the transistor reaches a thermal steady-state. The transient thermal impedance waveform is calculated, based on the measured V_{GS} voltage waveform, the measured value of the power dissipated in the transistor before the switch S_1 is closed, and the slope of the $V_{GS}(T)$ dependence.

The void ratio of the solder joints was measured using GE Sensing & Inspection Technologies Phoenix X-ray GmbH “Nanotom 180 N”. Mechanical cross-sections were fabricated from the solder joints to study their microstructure. The cross-sections were examined by a FEI Inspect S50 scanning electron microscopy (SEM) using a thermal emission gun and equipped with Bruker Quantax Energy-dispersive X-ray spectroscopy (EDS). The surface of the cross-sections was etched in some areas by Ga ion beam to enhance the contrast difference between the β -Sn grains by a Thermo Scientific Scios 2 type Focused Ion Beam (FIB) device. The etched areas were investigated by a Thermo Scientific Scios 2 type SEM having non-immersion field emission gun (FE) and with scanning ion microscopy (SIM) feature of the same device as well.

3. Results and discussions

Figs. 2 and 3 show the average transient thermal impedances of the samples. Differences were observed between the sample types in the saturation phase of the Z_{th} curves (after 10 s of the measurement). Before 10 s, the smaller differences were only measurement errors. The thermal impedance was the lowest in the case of 0.5 wt% of SiC nano-particles SAC-0.5SiC(p) (Fig. 3). All other SiC composite soldered samples showed higher Z_{th} values than the reference. Differences were found between the nano-particles and nano-fibers samples in favor of the nano-particles.

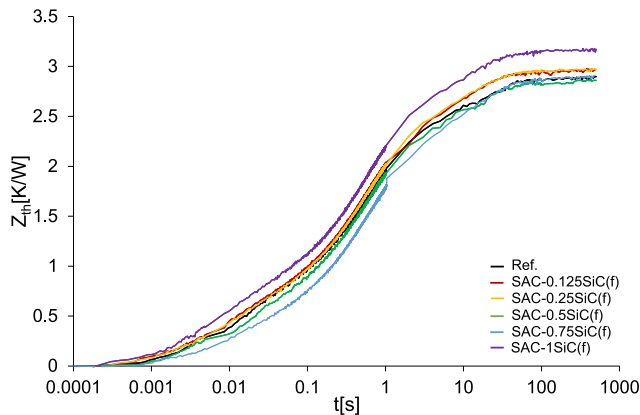


Fig. 2 – Average transient thermal impedances of the samples with SiC nano-fibers.

Fig. 4 presents the change of the average R_{th} values in the function of the SiC addition into the SAC0307 solder paste. As in the case of the Z_{th} values, only the samples with 0.5 wt% SiC nano-phases have better R_{th} (which means a lower value here) than the reference. SiC nano-particles in 0.5 wt% caused 5% R_{th} drop compared to the reference. In the case of 0.5 wt% SiC nano-fibers the decrease was only 1%. It suggests that from the point of thermal behavior of the MOSFET circuit, there is an optimal amount of SiC in the composite solder joints, around 0.5 wt%. This finding agrees with the previous results of El-Daly et al. [15], who got the best microstructural properties of SAC105 solder alloy with 0.35 wt% of SiC nano-particles, and with the results of Li et al. [29], who got the best wettability of Sn–xSiC/Cu solder with 0.6 wt% SiC nano-particles. The further increase of the SiC volume fraction in the solder pastes caused the deterioration of the microstructure and the wettability as well.

Since with both nano-phases (particles and fibers) the 0.5 wt% showed the best thermal parameters, during further investigations, the analysis was done only on those samples which contained 0.5 wt% SiC.

Fig. 5 Shows an example of the void ratios in the solder joint above the thermal pad. Solder joints reinforced with

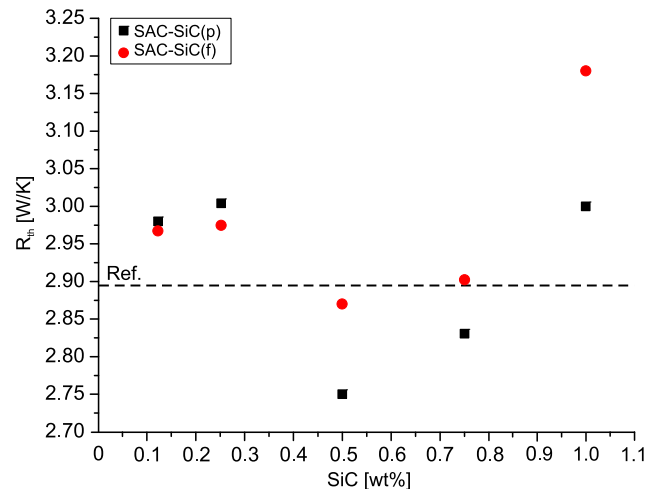


Fig. 4 – Average R_{th} values in the function of the SiC nano-phases' concentration in the composite solder joints.

0.5 wt% SiC nano-fibers had an average 21.00% ratio of voids (with SD 4.98%), while 0.5 wt% SiC powder showed an average of 12.50% (with SD 0.58%). Although these values are higher than the reference (having an average of 6.50% with 1.37% SD.), they are still under the acceptable 25–30% by IPC.

The gas voids in the solder joints naturally increase the thermal and electrical resistance of the solder joints since they could act like thermal-electrical insulation. Despite the much higher void ratio of the 0.5 wt% SiC composite solder joints, they provided the same or better Z_{th} and R_{th} values than the reference SAC0307 solder joints. It suggests that microstructural improvement probably occurred, which could compensate for the adverse effects of the large voids on the thermal parameters in the composite solder joints.

Fig. 6 shows the results of the first microstructure examination. The first major difference between the sample was the amount of dispersed IMC particles in the solder bulk. Dispersed Cu_6Sn_5 and Ag_3Sn IMC particles are always located at the β -Sn grain boundaries [14]. The reference SAC (Fig. 6a) and the SAC-0.5SiC(f) (Fig. 6c) contained agglomerated Ag_3Sn islands in the solder bulk. This phenomenon was not typical in the SAC-0.5SiC(p) samples (Fig. 6e). The amount and the distribution of dispersed Cu_6Sn_5 IMC particles were similar in all samples. The second major difference between the samples was the size of the β -Sn grain. In the case of the reference SAC (Fig. 6b) and the SAC-0.5SiC(f) (Fig. 6d), relatively large β -Sn grains were found with 40–50 μm sizes. In the case of the SAC-0.5SiC(p) (Fig. 6e) samples, considerable grain refinement occurred, and grains with 4–5 μm sizes were observed.

The surface adsorption theory can explain the observed grain refinement. The SiC nano-particles do not wet the β -Sn, and do not form IMCs in the solder matrix during the solidification process. The SiC nano-particles increase the grain boundary fraction, which enhances the SiC nano-particle's segregation to the grain boundaries. The high surface free energy causes the microstructure refinement on solidified β -Sn grain surfaces through the matrix, which adsorbs the SiC nano-particles during the solidification process [37]. Note the

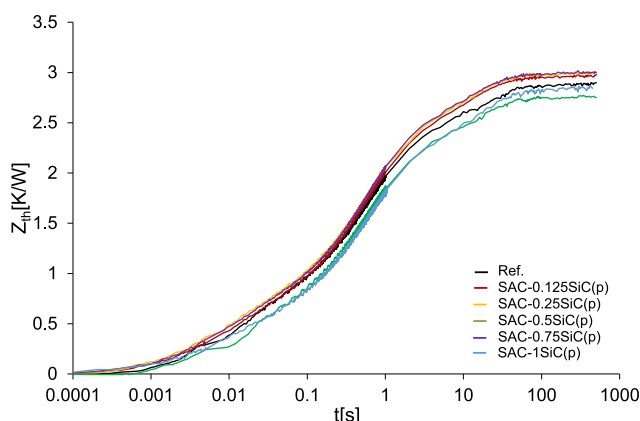


Fig. 3 – Average transient thermal impedances of the samples with SiC nano-particles.

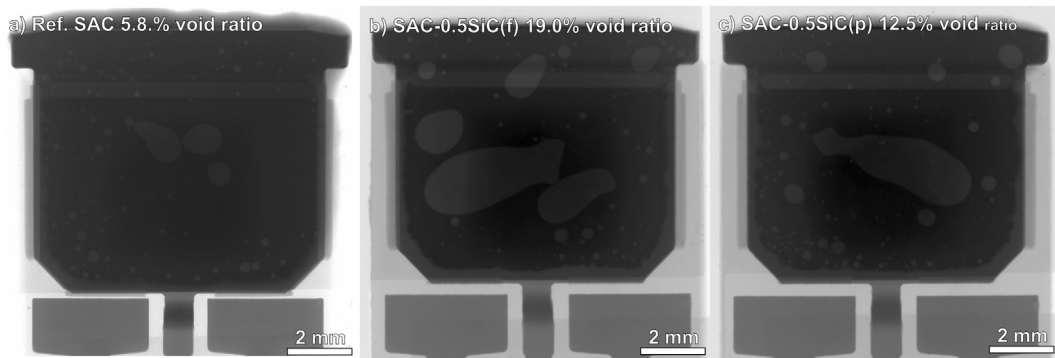


Fig. 5 – X-rays micrographs of the solder joints: (a) Ref.; (b) SAC-0.5SiC(f); (c) SAC-0.5SiC(p).

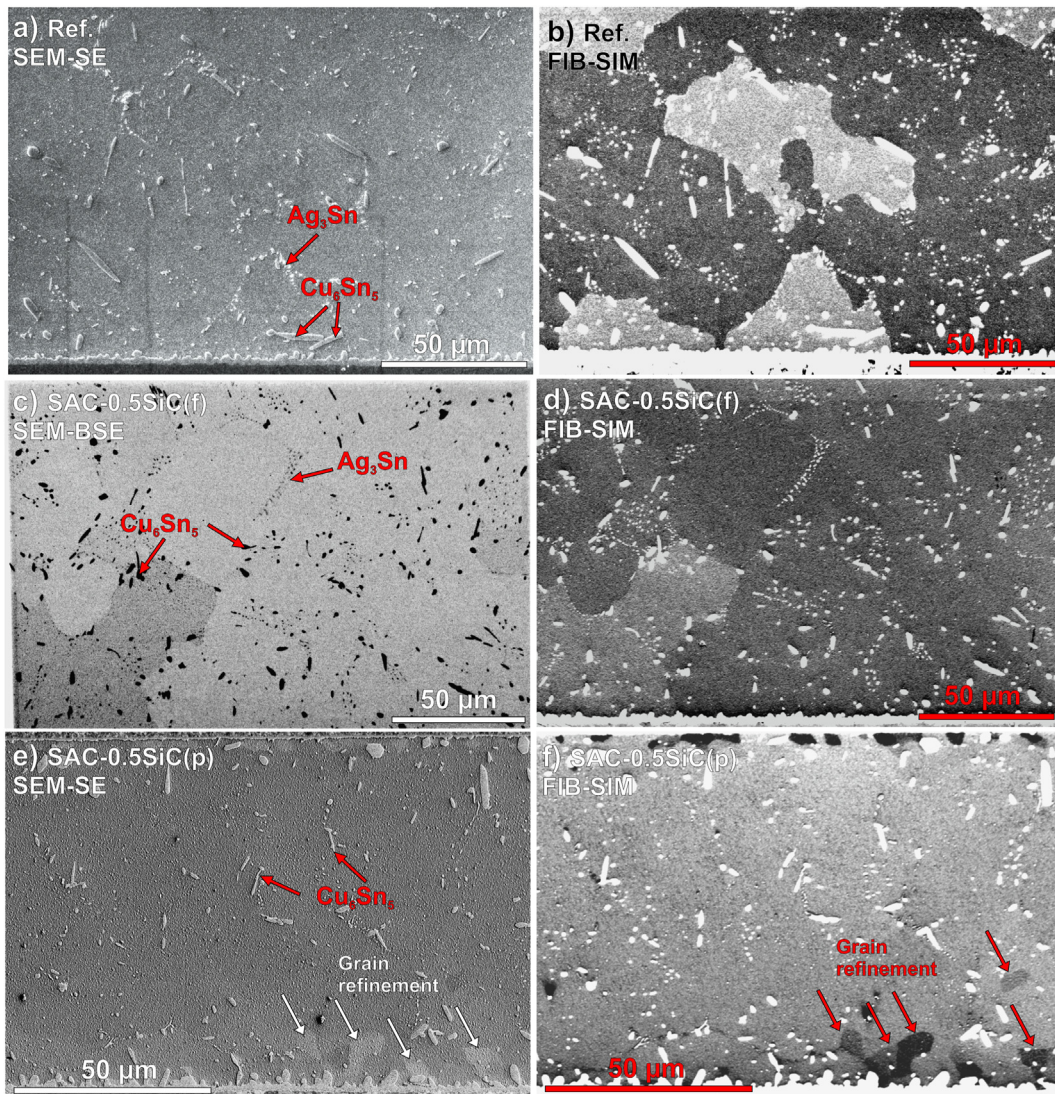


Fig. 6 – Microstructure examination of the solder joints: (a) SEM - SE Ref.; (b) FIB-SIM Ref.; (c) SEM-BSE SAC-0.5SiC(f); (d) FIB-SIM SAC-0.5SiC(f); (e) SEM - SE SAC-0.5SiC(p); (f) FIB-SIM SAC-0.5SiC(p).

orientation differences between the grains, which are well presented in the FIB-SIM micrographs by the contrast differences (Fig. 6).

Fig. 7 shows typical examples of the structure of IMC layers in the solder joints. In Fig. 7, M1-M6 represents the measurement areas of SEM-EDS, which helped to distinguish the different phases in the solder joints. The results can be found in Table 2. It has to be noted that in most of the measurement results, the Sn is overrepresented due to the very high weight fraction of Sn in the samples and the minimum sampling size limitation of the SEM-EDS. A solder joint contains two IMC layers between the component and the solder joint bulk

Table 2 – EDS measurement results from Fig. 7.

Measurement point/Element [at%]	Sn	Ag	Cu	Ni
M1 (Cu base)	0	0	100	0
M2 (Cu–Ni interface)	0	0	46.82	53.18
M3 (Solder bulk)	99.35	0.15	0.50	0
M4 (Cu_6Sn_5 IMC layer) ^a	50.66	0	40.69	8.65
M5 (Cu_6Sn_5 IMC particle)	76.52	0	22.64	0.84
M6 (Ag_3Sn IMC particles)	86.11	13.89	0	0

^a Ni was detectable in the IMC layer in a relatively high amount due to the closeness of the Ni barrier layer.

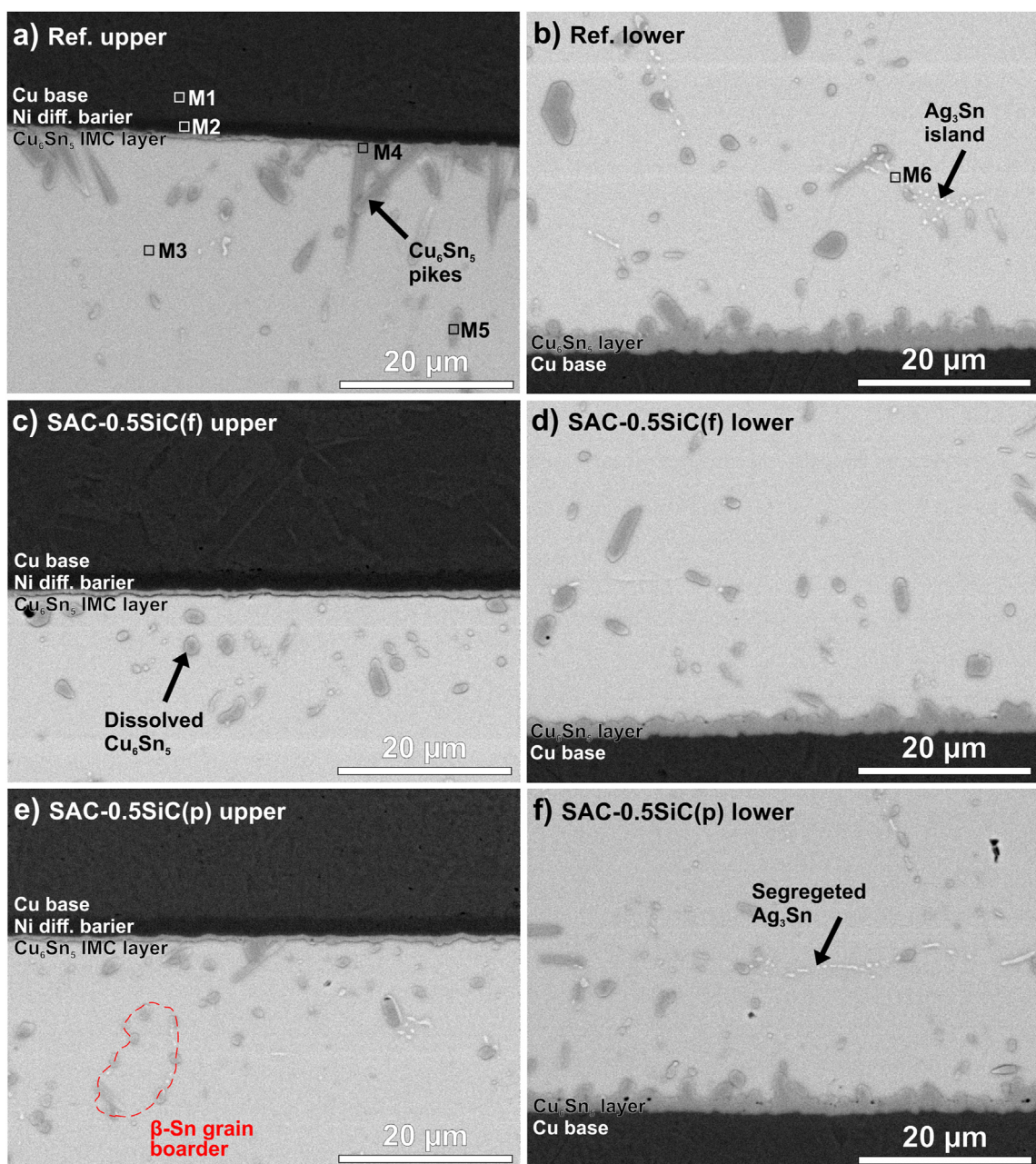


Fig. 7 – Structure of the IMC layers in the solder joints: (a) Ref. upper IMC layer; (b) Ref. lower IMC layer; (c) SAC-0.5SiC(f) upper IMC layer; (d) SAC-0.5SiC(f) lower IMC layer; (e) SAC-0.5SiC(p) upper IMC layer; (f) SAC-0.5SiC(p) lower IMC layer.

(upper one) and between the solder bulk and the substrate (lower one). The structure of the solder joints can be described “a sandwich” structure. The upper part meant the interface between the component (transistor) and the solder joint, the bottom part corresponded to the interface between the solder joint and the substrate. The upper IMC layers were always much thinner and more even than the lower ones.

The lower one was scallop type in all cases. It was caused by the different surface finishes on the component and the metal core printed circuit board (MCPCB). The component had Ni/Au layer as a diffusion barrier layer on the Cu base, which blocked the diffusion of Cu atoms during the formation of the solder joints, and this resulted in the thin upper IMC layer. The MCPCB had organic solderability preservatives (OSP) surface finish, which means a simple passivated Cu surface. This was dissolved during the solder joint formation, and the Cu atoms could diffuse freely from the Cu wiring into the solder joint.

In the reference SAC solder joints, frequently long Cu_6Sn_5 IMC pikes started from the upper IMC layer towards the solder bulk (Fig. 7a). In the case of the composite solder joints, this phenomenon was rare (Fig. 7c and e) since the nano-phases limit the grain growth in the liquid phase of the solder. In Fig. 7.b, the agglomeration of the dissolved Ag_3Sn can be observed at a $\beta\text{-Sn}$ grain boundary. On the contrary, well-segregated Ag_3Sn particles were observed in the composite solder joints, mainly in the SAC-0.5SiC(p) samples (Fig. 7e-f). During the solidification process, the SiC nano-phases ensure a high nucleation density of the second phase in the eutectic colony [38]. This and the refined $\beta\text{-Sn}$ matrix could cause the segregation of the Ag_3Sn IMC particles in SAC-0.5SiC(p) solder joints. Chuang et al. [39] and Tsao et al. [12] observed the same phenomenon using TiO_2 and Al_2O_3 nano-particles in SAC solder alloys. In the case of the SAC-0.5SiC(p) sample, even the $\beta\text{-Sn}$ grain refinement is visible in Fig. 7. e. The dispersed IMC particles are always located at the $\beta\text{-Sn}$ grain boundaries, indicating the boundaries well [14]. The red dashed line shows the boundary of a $\beta\text{-Sn}$ grain in Fig. 7. e.

Fig. 8 presents the statistical results of the IMC thickness values with box plots. The small squares represent the average, the horizontal lines indicate the median, the borders of the boxes indicate the $\pm\sigma$ standard deviation, and the crosses mark the min–max values. The addition of SiC nano-fibers and nano-particles suppressed the IMC layer growth in these solder joints. The upper average IMC layer thickness decreased from 0.67 μm to 0.51 μm and to 0.59 μm , which means a 23% and a 12% decrease (SiC nano-fibers and nano-particles, respectively). The lower average IMC layer thickness decreased from 3.32 μm to 2.60 μm and to 2.51 μm , which means a 22% and a 24% decrease (SiC nano-fibers and nano-particles, respectively). The thinner IMC layers in the composite solder joints were formed due to the suppression of grain growth by the SiC ceramic particles during the liquid phase of the solder alloy. Minor statistical differences were found only between the decreasing ratios of the upper IMC layers in favor of SiC nano-fibers. However, this could probably be a measurement artifact caused by the increasing inaccuracy of the IMC thickness measurement in the sub-micron range.

The interfacial growth model of the Cu_6Sn_5 IMC layer is the following: the liquid solder is considered a binary solution system, in which Cu is solute and Sn is solvent. The

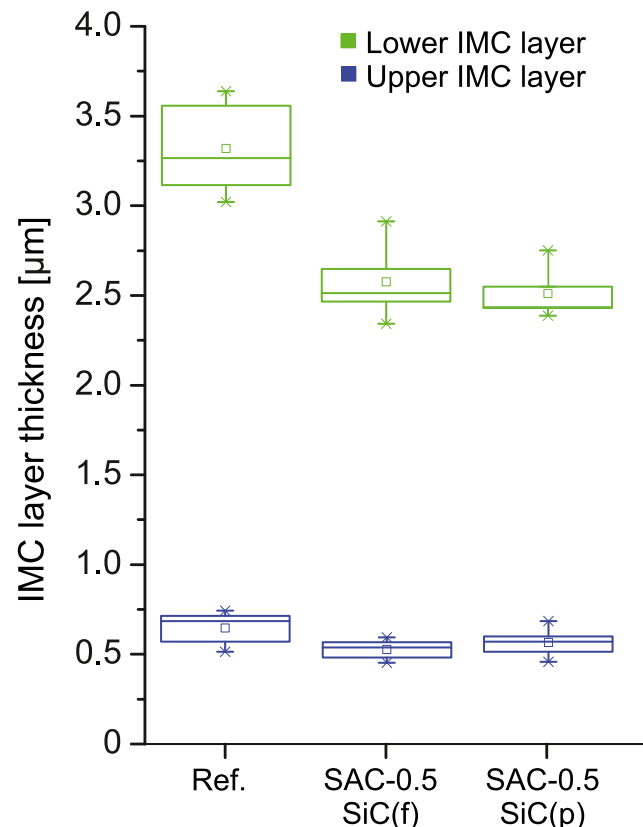


Fig. 8 – Thickness statistics of the IMC layers at the lower and upper Cu/Sn interfaces in 0.5 wt% SiC composite alloys.

distribution of Cu inside the liquid solder is determined by the Gibbs–Thomson effect, which can be expressed at the solid/liquid interface as [40]:

$$C_r = C_0 \cdot e^{(2\gamma\Omega/rRT)} \quad (1)$$

where C_0 is the equilibrium concentration of Cu in the liquid solder, C_r is the concentration of Cu in the liquid solder at the surface of the Cu_6Sn_5 grain, γ is the interfacial energy per unit area between Cu_6Sn_5 and molten solder, Ω is the molar volar volume of Cu_6Sn_5 , r is the radius of (size) of Cu_6Sn_5 grain, T is the temperature, and R is the gas constant. According to Eq. (1), the Cu concentration at the surface of a Cu_6Sn_5 grain (C_r) depends on its' radius (r). The smaller Cu_6Sn_5 grains have higher C_r at their' interface. So the different Cu_6Sn_5 sizes cause the gradient of C_r . The concentration difference of Cu gives the driving force for the diffusion of Cu during the soldering, and this initiates the growth of Cu_6Sn_5 grains. It can be assumed that C_0 is near the same everywhere inside the liquid solder. Therefore there is no driving force for the diffusion of Cu inside the liquid solder [40].

The flux of the Cu_6Sn_5 phase formation in the interface reaction can be given as follows:

$$J_{\text{Cu}_6\text{Sn}_5} = J_{\text{SAC}} + J_{\text{IMC}} - J_{\text{SAC/IMC}} + J_R \quad (2)$$

where J_{SAC} is the diffusion flux of Cu into liquid solder through the boundary of Cu_6Sn_5 grains, J_{IMC} is the bulk diffusion flux of

Cu into Cu_6Sn_5 grains from the substrate, $J_{\text{SAC/IMC}}$ is the diffusion flux of Cu into liquid solder through the top surface of Cu_6Sn_5 grains, and J_R is the diffusion flux of Cu due to the Cu_6Sn_5 grain size differences [40]. However, in the composite solders, the dispersed SiC nano-phases in the molten solder appear on the Sn–Cu interface of the solder joints and modify the Cu_6Sn_5 grain growth. Fig. 9 shows the SiC nano-particles presence at the Sn–Cu interface on the surface of the Cu_6Sn_5 IMC layer.

The presence of SiC nano-phases can have two effects on Cu_6Sn_5 grain growth. First, they decrease the thermodynamic energy of Cu_6Sn_5 nucleation since the Cu_6Sn_5 prefers to nucleate on the SiC nano-phases (according to the heterogeneous nucleation theory). Compared to their relatively low volume fraction, the very high number of the SiC nano-phases inducing many nucleation sites results in a higher nucleation probability of Cu_6Sn_5 grain growth. This enhances the nucleation rate and causes the refinement of the Cu_6Sn_5 grain structure by blocking the sequential grain ripening. Furthermore, the decrease of Cu_6Sn_5 IMC layer thickness could also be caused by the adsorption of SiC nano-phases as a surface-active material. The surface energy of the Cu_6Sn_5 grains is minimized in the equilibrium state. The adsorption of an active element like SiC nano-phases decreases this surface energy. The reduction of the surface energy reduces the growth of the Cu_6Sn_5 grains and results in a suppression effect on the Cu_6Sn_5 IMC layer growth [14].

After the solidification, the SiC nano-phases in the solder bulk act as diffusion barriers of Sn and Cu atoms. This further suppresses the Cu_6Sn_5 IMC layer growth in the solidified joint; since diffusion becomes the dominant phenomenon in the further development of the IMC layer. The Cu_6Sn_5 IMC thickness could also be decreased by the spalling of the IMCs into the solder bulk [41,42]. Tang et al. [41] found that the incorporated TiO_2 nano-phases at the IMC grain boundaries can cause the intensive spalling/braking of the IMCs in the composite solder joints. However, in our case with SiC nano-phases, considerable spalling of the IMC layer was not detected.

Consequently, the application of 0.5 wt% SiC nano-phases resulted in considerable changes in the microstructure of the

solder joints. The SiC nano-particles in 0.5 wt% decreased the number and the sizes of the agglomerated Ag_3Sn in the solder bulk, refined the $\beta\text{-Sn}$ grains by one order of magnitude and decreased the IMC layer thickness at the substrate side by 25%. In the case of the SiC nano-fibers, only a decrease in the IMC layer thicknesses was observed. The thermal parameters (Figs. 2–4, Z_{th} and R_{th}) correlated with the IMC layer thicknesses (Fig. 8). The lowest Z_{th} and R_{th} values were measured in the case of 0.5 wt% SiC nano-particles addition, in which samples, the thinnest IMC layers (bottom and upper together) were detected. This can be explained by the specific thermal conductivity of the bulk SnAgCu solders, which is double (55–60 W/mK [43]) as the same parameter of Cu_6Sn_5 IMC (34 W/mK [44]). In the case of 0.5 wt% SiC nano-fibers addition, probably even the suppressed IMC layers could not compensate for the negative effect of the much higher amount of large gas voids in the joints.

4. Conclusions

The effect of SiC nano-particles and nano-fibers addition into SAC0307 solder paste on the thermal and microstructural properties of the composite solder joints was investigated. It was found that the SiC nano-phases improved the thermal parameters of the investigated MOSFET assembly but only in the case of 0.5 wt% addition. Despite the nano-phases increased the void formation in the solder joints. Any other amount of SiC nano-phases resulted in slightly worst or similar thermal parameters than the samples soldered with the reference SAC0307 alloy. It was proven that not only from the wettability or the microstructure but from the point of thermal behavior as well, the optimal amount of SiC in the composite solder joints is around 0.5 wt%. The SiC nano-particles resulted in considerable changes in the microstructure of the solder joints. It decreased the spacing and the amount of agglomerated Ag_3Sn in the solder bulk, refined the $\beta\text{-Sn}$ grains and suppressed the IMC layer thickness. In the case of the SiC nano-fibers, only a decrease in the IMC layer thicknesses was observed. The thinner IMC layers could

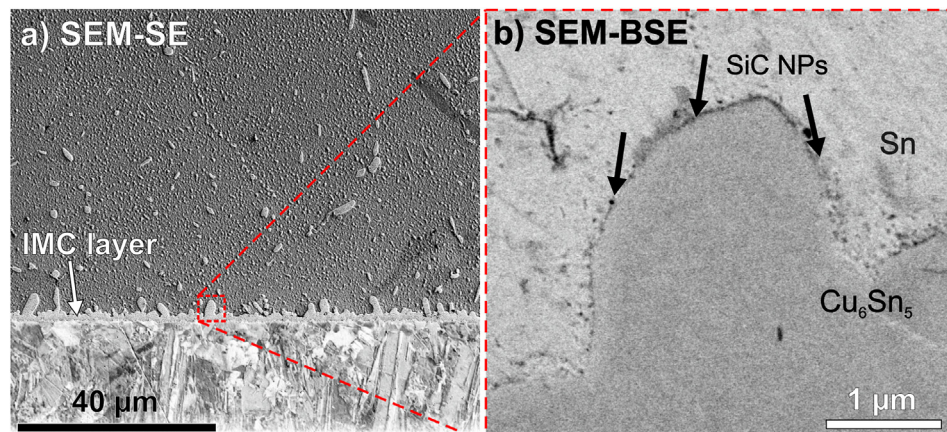


Fig. 9 – SiC nano-particles on the Cu_6Sn_5 IMC layer: (a) SEM - SE micrograph about the investigated area; (b) highly magnified SEM-BSE micrograph of the SiC nano-particles incorporation.

explain the better thermal parameters of the composite solder joints since the SnAgCu solder alloys have better specific thermal conductivity than the Cu₆Sn₅ IMC. Better thermal parameters of the SiC composite solder joints could be achieved by decreasing the voids in them. Generally, the application of SiC nano-particles for soldering power electronics is suggested, but only in around 0.5 wt% amount.

Declaration of Competing Interest

The authors declare the following financial interests/personal relationships which may be considered as potential competing interests: Agata Skwarek reports financial support was provided by Łukasiewicz Research Network-Institute of Microelectronics and Photonics, Zablocie 39, 30–701 Kraków, Poland.

Acknowledgment

This study was partially supported by the Ministry of Science and Higher Education—Poland (MNiSW) as part of project No. 006/RID/2018/19 financed by the program “Regionalna Inicjatywa Doskonalosci 2019–2022”, the amount provided is 11 870 000 PLN and by the National Research Development and Innovation Office – Hungary (NKFIH) as part of Project Number FK 127970.

REFERENCES

- [1] El-Daly AA, Elmosalami TA, Desoky WM, El-Shaarawy MG, Abdraboh AM. Tensile deformation behavior and melting property of nano-sized ZnO particles reinforced Sn–3.0 Ag–0.5 Cu lead-free solder. *Mater Sci Eng, A* 2014;618:389–97.
- [2] El-Daly AA, Fawzy A, Mansour SF, Younis MJ. Thermal analysis and mechanical properties of Sn–1.0 Ag–0.5 Cu solder alloy after modification with SiC nano-sized particles. *J Mater Sci Mater Electron* 2013;24:2976–88.
- [3] Salleh MM, McDonald S, Nogita K. Effects of Ni and TiO₂ additions in as-reflowed and annealed Sn0.7Cu solders on Cu substrates. *J Mater Process Technol* 2017;242:235–45.
- [4] Ani FC, Jalar A, Saad AA, Khor CY, Ismail R, Bachok Z, et al. SAC–xTiO₂ nano-reinforced lead-free solder joint characterizations in ultra-fine package assembly. *Solder Surf Mt Technol* 2018;30:1–13.
- [5] Gain AK, Chan Y, Yung WK. Effect of additions of ZrO₂ nanoparticles on the microstructure and shear strength of Sn–Ag–Cu solder on Au/Ni metallized Cu pads. *Microelectron Reliab* 2011;51:2306–13.
- [6] Gain AK, Zhang L. Microstructure, mechanical and electrical performances of zirconia nanoparticles-doped tin-silver-copper solder alloys. *J Mater Sci Mater Electron* 2016;27:7524–33.
- [7] Chen G, Liu L, Silberschmidt VV, Chan Y, Liu C, Wu F. Retained ratio of reinforcement in SAC305 composite solder joints: effect of reinforcement type, processing and reflow cycle. *Solder Surf Mt Technol* 2016;28:159–66.
- [8] Tang Y, Li G, Pan Y. Effects of TiO₂ nanoparticles addition on microstructure, microhardness and tensile properties of Sn–3.0Ag–0.5Cu–xTiO₂ composite solder. *Mater Des* 2014;55:574–82.
- [9] Ramli M, Saud N, Salleh MM, Derman MN, Said RM, Izwan MI. Effect of TiO₂ additions on Sn–0.7Cu–0.05Ni lead-free composite solder. *Microelectron Reliab* 2016;65:255–64.
- [10] Zhang P, Xue S, Wang J, Xue P, Zhong S, Long W. Effect of nanoparticles addition on the microstructure and properties of lead-free solders: a review. *Appl Sci* 2019;9:2044.
- [11] Tan AT, Yusof F. Influence of nanoparticle addition on the formation and growth of intermetallic compounds (IMCs) in Cu/Sn–Ag–Cu/Cu solder joint during different thermal conditions. *Sci Technol Adv Mater* 2015;16:33505.
- [12] Tsao L, Chang S. Effects of Nano-TiO₂ additions on thermal analysis, microstructure and tensile properties of Sn–3.5Ag0.25Cu solder. *Mater Des* 2010;31:990–3.
- [13] Eid EA, Fouada AN, Duraia ESM. Effect of adding 0.5 wt% ZnO nanoparticles, temperature and strain rate on tensile properties of Sn–5.0 wt% Sb–0.5 wt% Cu (SSC505) lead free solder alloy. *Mater Sci Eng* 2016;657:104–14.
- [14] Skwarek A, Krammer O, Hurtony T, Ptak P, Górecki K, Wroński S, et al. Application of ZnO nanoparticles in Sn99Ag0.3Cu0.7 based composite solder alloys. *Nanomaterials* 2021;11:1545.
- [15] El-Daly A, Al-Ganainy G, Fawzy A, Younis M. Structural characterization and creep resistance of nano-silicon carbide reinforced Sn–1.0Ag–0.5Cu lead-free solder alloy. *Mater Des* 2014;55:837–45.
- [16] Shi Y, Liu J, Xia Z, Lei Y, Guo F, Li X. Creep property of composite solders reinforced by nano-sized particles. *J Mater Sci Mater Electron* 2007;19:349–56.
- [17] Salleh MAAM, Al Bakri AMM, Kamarudin H, Bnhussain M, Somidin F. Solderability of Sn–0.7Cu/Si3N4 lead-free composite solder on Cu-substrate. *Phys Procedia* 2011;22:299–304.
- [18] Fawzy A, Fayek S, Sobhy M, Nassr E, Mousa M, Saad G. Tensile creep characteristics of Sn–3.5Ag–0.5Cu (SAC355) solder reinforced with nano-metric ZnO particles. *Mater Sci Eng* 2014;603:1–10.
- [19] Yang X, Yang X, Kawai K, Arima K, Yamamura K. Novel SiC wafer manufacturing process employing three-step slurryless electrochemical mechanical polishing. *J Manuf Process* 2021;70:350–60.
- [20] Han S, Yu H, He C, Zhao S, Ning C, Jiang L, et al. Laser slicing of 4H-SiC wafers based on picosecond laser-induced micro-explosion via multiphoton processes. *Opt Laser Technol* 2022;154:108323.
- [21] Liu P, Yao P, Liu J. Effect of SiC nanoparticle additions on microstructure and microhardness of Sn–Ag–Cu solder alloy. *J Electron Mater* 2008;37:874–9.
- [22] Wang X, Liu YC, Wei C, Gao HX, Jiang P, Yu LM. Strengthening mechanism of SiC-particulate reinforced Sn–3.7Ag–0.9Zn lead-free solder. *J Alloys Compd* 2009;480:662–5.
- [23] El-Daly AA, Desoky WM, Elmosalami TA, El-Shaarawy MG, Abd Raboh AM. Microstructural modifications and properties of SiC nanoparticles-reinforced Sn–3.0Ag–0.5Cu solder alloy. *Mater Des* 2015;65:1196–204.
- [24] El-Daly AA, Fawzy A, Mansour SF, Younis MJ. Novel SiC nanoparticles-containing Sn–1.0Ag–0.5Cu solder with good drop impact performance. *Mater Sci Eng* 2013;578:62–71.
- [25] Kim Y, Nagao S, Sugahara T, Suganuma K, Ueshima M, Albrecht HJ, et al. Refinement of the microstructure of Sn–Ag–Bi-in solder, by addition of SiC nanoparticles, to reduce electromigration damage under high electric current. *J Electron Mater* 2014;43:4428–34.
- [26] Wu B, Leng X, Xiu Z, Yan J. Microstructural evolution of SiC joints soldered using Zn–Al filler metals with the assistance of ultrasound. *Ultrason Sonochem* 2018;44:280–7.

- [27] Pal MK, Gergely G, Koncz-Horváth D, Gácsi Z. Investigation of the electroless nickel plated SiC particles in SAC305 solder matrix. *Powder Metall Met Ceram* 2020;58:529–37.
- [28] Pal MK, Gergely G, Koncz-Horváth D, Gácsi Z. Characterization of the interface between ceramics reinforcement and lead-free solder matrix. *Surface Interfac* 2020;20:100576.
- [29] Li M, Zhang L, Jiang N, Zhong S, Zhang L. Influences of silicon carbide nanowires' addition on IMC growth behavior of pure Sn solder during solid–liquid diffusion. *J Mater Sci Mater Electron* 2021;32:18067–75.
- [30] Li M, Gao L, Zhang L, Long W, Zhong S, Zhang L. Interfacial evolution of pure Sn solder bearing silicon carbide nanowires under isothermal aging and thermal cycling. *J Mater Res Technol* 2021;15:3974–82.
- [31] Yin L, Zhang Z, Su Z, Zhang H, Zuo C, Yao Z, et al. Interfacial microstructure evolution and properties of Sn–0.3Ag–0.7Cu– x SiC solder joints. *Mater Sci Eng, A* 2021;809: 140995.
- [32] Pal MK, Gergely G, Koncz-Horváth D, Gácsi Z. Investigation of microstructure and wetting behavior of Sn–3.0Ag–0.5Cu (SAC305) lead-free solder with additions of 1.0 wt % SiC on copper substrate. *Intermetallics* 2021;128:106991.
- [33] Goldberg Y, Levinshtein ME, Rumyantsev SL. In: Levinshtein ME, Rumyantsev SL, Shur MS, editors. *Properties of advanced SemiconductorMaterials GaN, AlN, SiC, BN, SiC, SiGe*. Eds. New York: John Wiley & Sons; 2001. p. 93–148.
- [34] Momohjimoh I, Hussein MA, Al-Aqeeli N. Recent advances in the processing and properties of alumina–CNT/SiC nanocomposites. *Nanomaterials* 2019;9:86.
- [35] Parchovianský M, Galusek D, Švancárek P, Sedláček J, Šajgalík P. Thermal behavior, electrical conductivity and microstructure of hot pressed Al₂O₃/SiC nanocomposites. *Ceram Int* 2014;40:14421–9.
- [36] Górecki P, Górecki K. Measurements and computations of internal temperatures of the IGBT and the diode situated in the common case. *Electronics* 2021;10:210.
- [37] El-Rehim AFA, Zahran HY, Yassin AM. Microstructure evolution and tensile creep behavior of Sn–0.7Cu lead-free solder reinforced with ZnO nanoparticles. *J Mater Sci Mater Electron* 2018;30:2213–23.
- [38] Chang SY, Tsao LC, Wu MW, Chen CW. The morphology and kinetic evolution of intermetallic compounds at Sn–Ag–Cu solder/Cu and Sn–Ag–Cu–0.5Al₂O₃ composite solder/Cu interface during soldering reaction. *J Mater Sci Mater Electron* 2012;23:100–7.
- [39] Chuang TH, Wu MW, Chang SY, Ping SF, Tsao LC. Strengthening mechanism of nano-Al₂O₃ particles reinforced Sn3.5Ag0.5Cu lead-free solder. *J Mater Sci Mater Electron* 2011;22:1021–7.
- [40] Qu L, Zhao N, Zhao HJ, Huang ML, Ma HT. In situ study of the real-time growth behavior of Cu₆Sn₅ at the Sn/Cu interface during the soldering reaction. *Scripta Mater* 2014;72–73:43–6.
- [41] Tang Y, Li GY, Pan YC. Influence of TiO₂ nanoparticles on IMC growth in Sn–3.0Ag–0.5Cu– x TiO₂ solder joints in reflow process. *J Alloys Compd* 2013;554:195–203.
- [42] Chen BL, Li GY. Influence of Sb on IMC growth in Sn–Ag–Cu–Sb Pb-free solder joints in reflow process. *Thin Solid Films* 2004;462–463:395–401.
- [43] Zhang Z, Cao H, Xiao Y, Cao Y, Li M, Yu Y. Electromigration-induced growth mode transition of anodic Cu₆Sn₅grains in Cu₃SnAg3.0Cu0.5jCu lap-type interconnects. *J Alloys Compd* 2017;703:1–9.
- [44] Frederikse HPR, Fields RJ, Feldman A. Thermal and electrical properties of copper-tin and nickel-tin intermetallics. *J Appl Phys* 1992;72:2879.